EPJ Web of Conferences will be set by the publisher
DOI: will be set by the publisher
© Owned by the authors, published by EDP Sciences, 2014

arXiv:1412.4243v1 [hep-ex] 13 Dec 2014

Recent results from NA61/SHINE

Marek Gazdzicki[1,2,a] for the NA61/SHINE Collaboration

[1] *Goethe–University, Frankfurt, Germany*
[2] *Jan Kochanowski University, Kielce, Poland*

Abstract. This paper briefly presents the NA61/SHINE facility at the CERN SPS and its measurements motivated by physics of strong interactions, neutrinos and cosmic rays.

1 Introduction

NA61/SHINE is a multi-purpose experimental facility to study hadron production in hadron-proton, hadron-nucleus and nucleus-nucleus collisions at the CERN Super Proton Synchrotron. Measurements motivated by physics of strong interactions, neutrinos and cosmic rays have been performed up to now. The first physics data with secondary hadron (protons, pions and kaons) beams were recorded in 2009 and with nuclear beams (secondary ^{7}Be beams) in 2011.

This contribution briefly presents the NA61/SHINE facility [1] in Sec. 2 and recent results [2] on the three physics programs in Secs. 3, 4, and 5. The contribution consists of copies of the slides presented at the conference *New Frontiers in Physics 2014* included as figures with captions.

[a] e-mail: marek@cern.ch

2 Facility

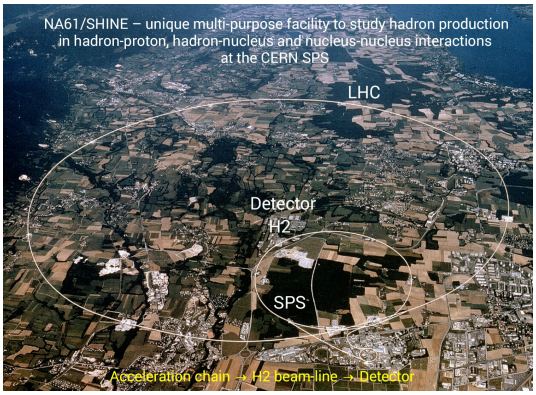

Figure 1. The NA61/SHINE facility is located at the European Organization for Nuclear Research, CERN, on the Franco-Swiss border near Geneva. The acceleration chain delivers proton and nuclear beams to the T2 target located in the North Area target cavern at the beginning of the H2 beam-line. Then the beams are either directly transported to the detector or used to produce secondary beams.

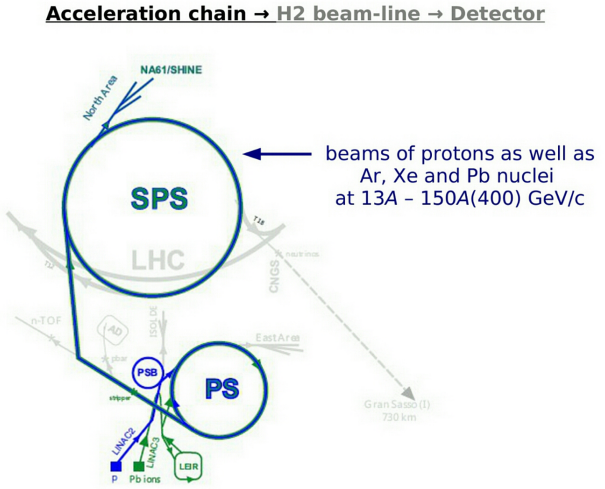

Figure 2. The proton and ion acceleration chains use different particle sources, linear accelerators (LINAC2 and LINAC3) and circular accumulator machines (PSB and LEIR). They share the Proton Synchrotron (PS) and the Super Proton Synchrotron (SPS).

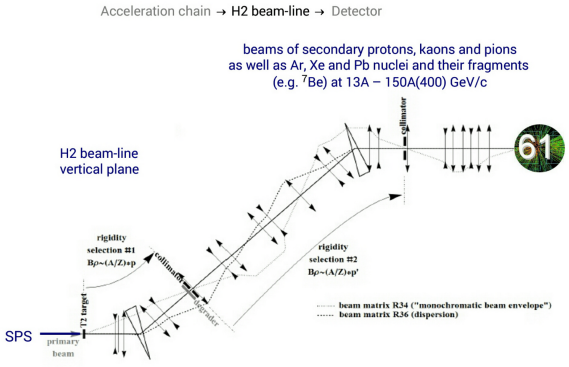

Figure 3. The beam extracted from the SPS is transported over about 1 km by bending and focusing magnets and then split into three parts each one directed towards a target where secondary beams can be created. The H2 beam-line emerges from the T2 primary target and is able to transport momentum selected secondary particles to the Experimental Hall North 1 where the detector is located. The physics target is at 535 m distance from the T2 target. The H2 beam-line can transport charged particles in a wide range of momenta from ~ 9 GeV/c up to the top SPS energy of 400 GeV/c. Alternatively it can transport a primary beam of protons or nuclei. The momentum selection is done in the vertical plane. The beam-line basically consists of two long spectrometers.

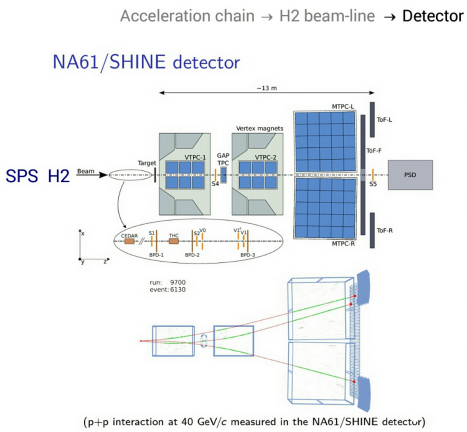

Figure 4. The NA61/SHINE detector consists of a large acceptance hadron spectrometer with excellent capabilities in charged particle momentum measurements and identification by a set of six Time Projection Chambers as well as Time-of-Flight detectors. The high resolution forward calorimeter, the Projectile Spectator Detector, measures energy flow around the beam direction, which in nucleus-nucleus reactions is primarily a measure of the number of spectator (not taking part in the interaction) nucleons and thus related to the volume of interacting matter. For hadron-nucleus interactions, the collision volume is determined by counting low momentum particles emitted from the nuclear target with the LMPD detector (a small TPC) surrounding the target. An array of beam detectors identifies beam particles, secondary hadrons and nuclei as well as primary nuclei, and measures precisely their trajectories.

3 Strong interactions

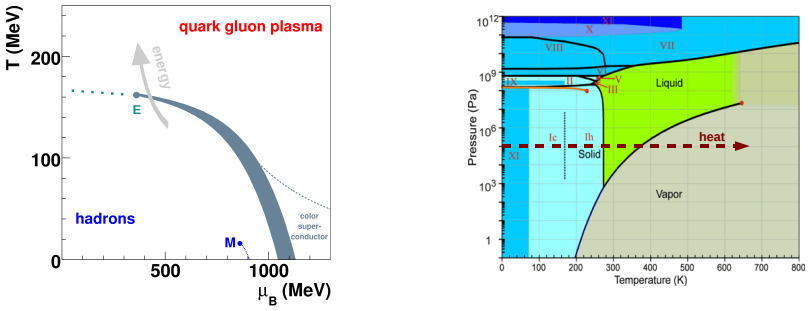

Figure 5. The NA61/SHINE measurements for physics of strong interactions are motivated by the question what happens when strongly interacting matter gets hotter/denser and its volume increases. In particular, the structure of the transition domain between matter consisting of hadrons and quark gluon plasma (see the left plot) is under study. How the signals of the onset of deconfinement observed in central Pb+Pb collisions collisions [3] are modified when decreasing the size of colliding nuclei? Is the structure of the transition line similar to the one of water (see the right plot) with the critical point separating the first order phase transition from the cross-over?

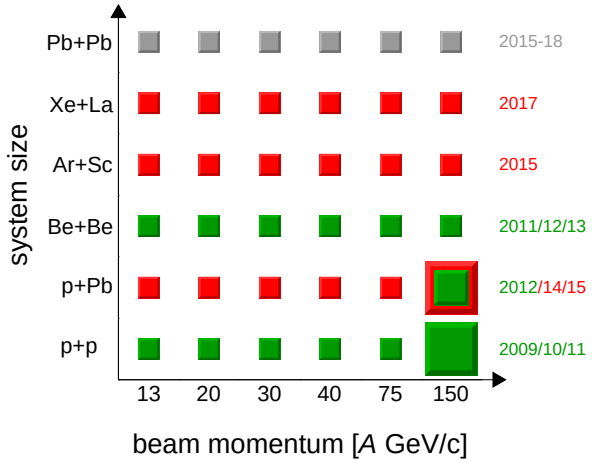

Figure 6. For the programme on strong interactions NA61/SHINE scans in the system size and beam momentum. In the plot the recorded data are indicated in green, the approved future data taking in red, whereas the proposed extension for the period 2015–2018 in gray.

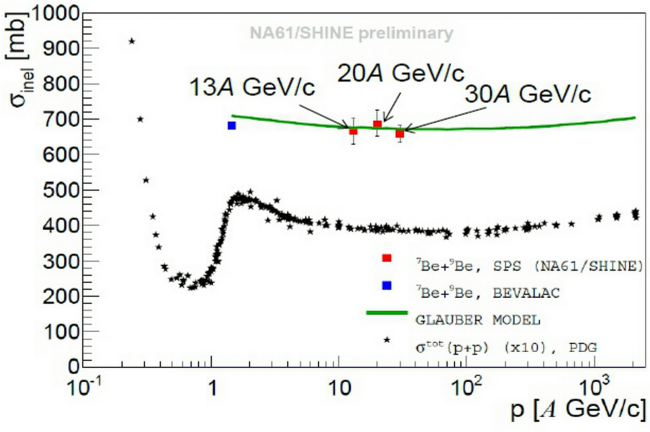

Figure 7. The inelastic cross section for ^{7}Be+^{9}Be collisions is weakly dependent on collision energy above 2A GeV. It is well reproduced by the Glissando version of the Glauber model [4].

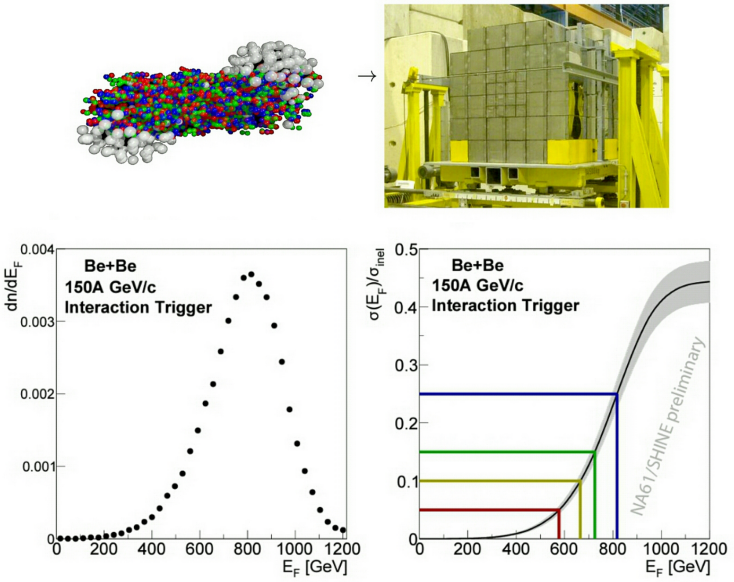

Figure 8. The selection of the reaction volume in ^{7}Be+^{9}Be collisions is performed by dividing recorded events into four classes according to the forward (mostly projectile spectator) energy, E_F, measured by the Projectile Spectator Detector (see the top plots). The first class comprises 5% of all inelastic collisions with the smallest E_F and the next classes 5-10%, 10-15% and 15-20%, respectively (see the bottom plots).

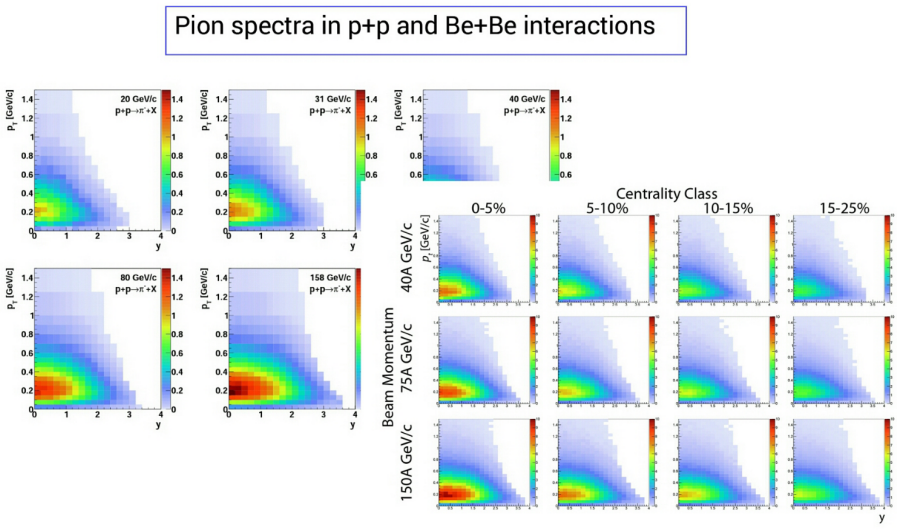

Figure 9. Negatively charged pion spectra are measured in inelastic p+p interactions [5] and volume selected ^{7}Be+^{9}Be collisions in the SPS energy range. High statistics and large acceptance allow to obtain two-dimensional (rapidity-transverse momentum) distributions.

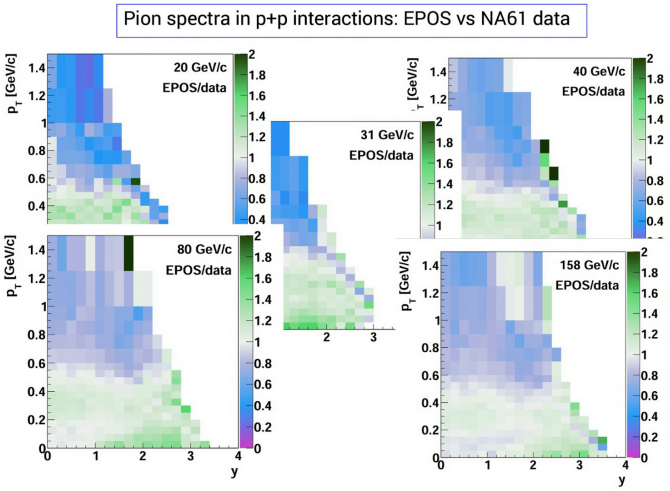

Figure 10. Negatively charged pion spectra measured in inelastic p+p interactions [5] are used to fit basic parameters of string-resonance models [6–11] and test scaling ideas [12].

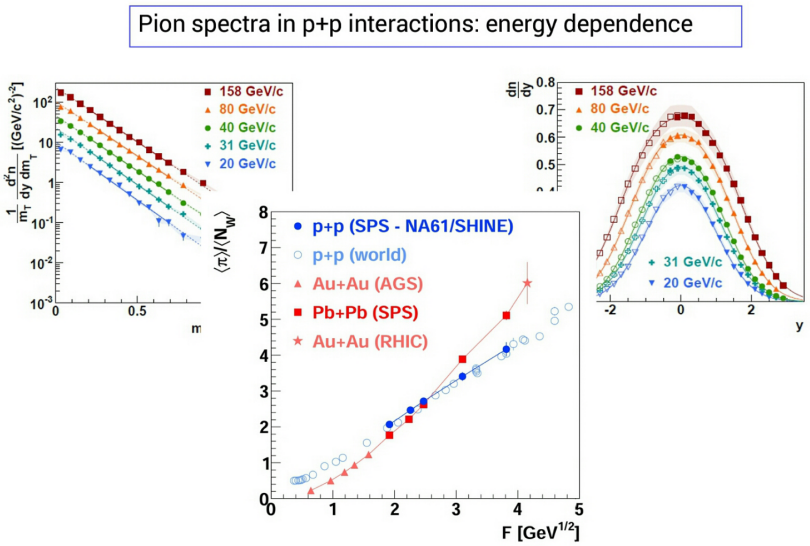

Figure 11. Collision energy dependence is studied by making slices, projections and integrals of the two-dimensional spectra. Examples are given for negatively charged pions: transverse mass spectra at mid-rapidity (top, left), rapidity spectra (top right) and mean pion multiplicity per wounded nucleon (bottom) [5].

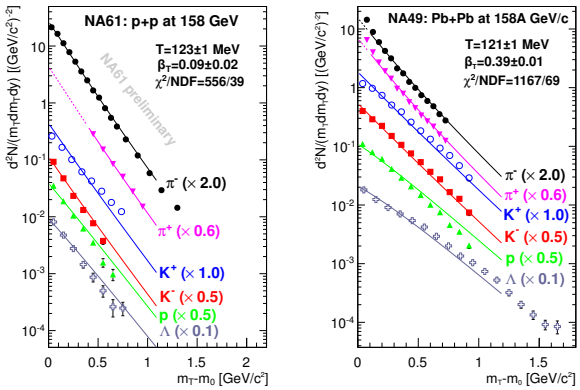

Figure 12. Mid-rapidity transverse mass spectra of various measured particle species are approximately exponential in inelastic p+p interactions at 158 GeV/c. In central Pb+Pb collisions at 158*A* GeV/c [13, 14] large deviations from the exponential dependence are observed. It is common to attribute this finding to the transverse collective flow which is expected to increase with increasing volume of the colliding matter and collision energy.

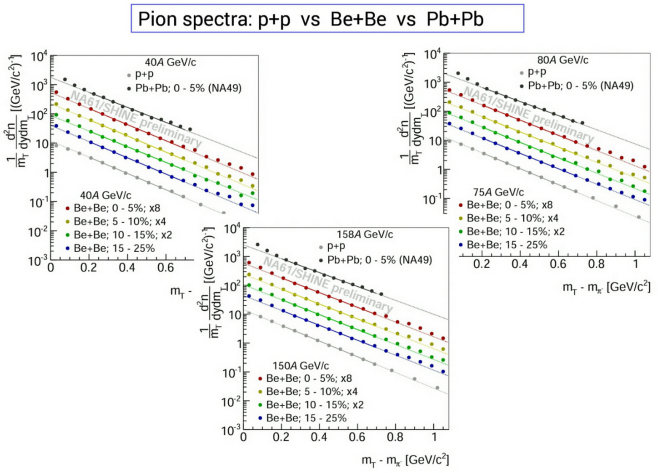

Figure 13. Mid-rapidity transverse mass spectra of negatively charged pions measured in inelastic p+p interactions as well as volume selected Be+Be and Pb+Pb collisions are compared at 40A, 75(80)A and 150(158)A GeV/c. An exponential function with the inverse slope parameter T is fitted in the interval $0.2 < m_T - m_\pi < 0.7$ GeV (shown by lines).

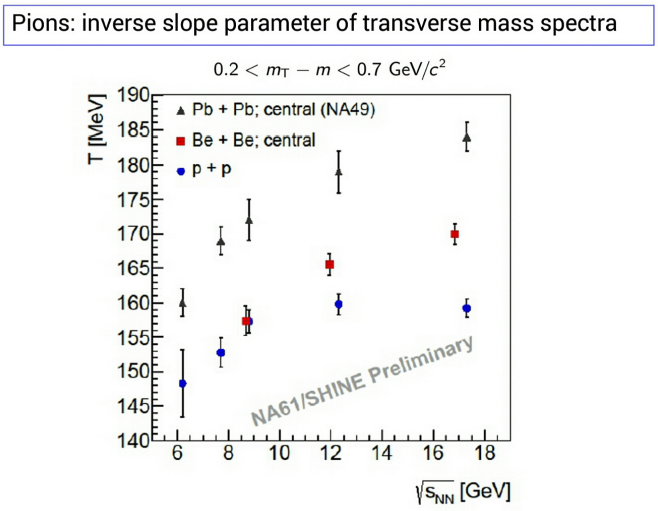
Pions: inverse slope parameter of transverse mass spectra
0.2 < m_T − m < 0.7 GeV/c²
Pb + Pb; central (NA49)
Be + Be; central
p + p
NA61/SHINE Preliminary
T [MeV]
√s_NN [GeV]

Figure 14. The T parameter increases with increasing collision energy for all studied reactions. In large volume Pb+Pb collisions T is larger than in p+p interactions. The results for large volume Be+Be collisions, T(p+p) < T(Be+Be) < T(Pb+Pb) at 75A and 150A GeV/c, and T(Be+Be)≈T(p+p) at 40A GeV/c, suggest that the collective flow is significant in Be+Be collisions at the high SPS beam momenta and gets reduced at 40A GeV/c.

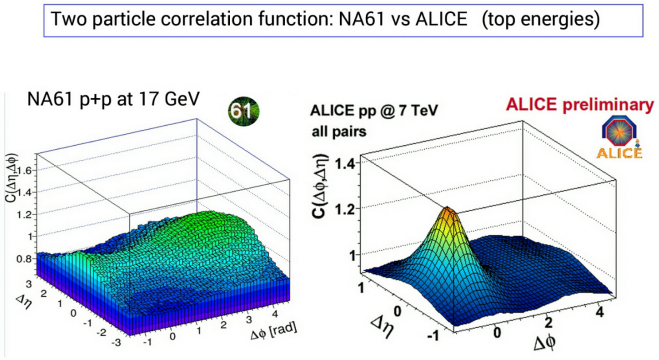

Figure 15. The two-particle correlation function in pseudo rapdity and azimuthal angle in inelastic p+p interactions is very different at the SPS and LHC energies. In particular, the saddle at (0,0) observed at the SPS is changed to the pronounced peak at the LHC.

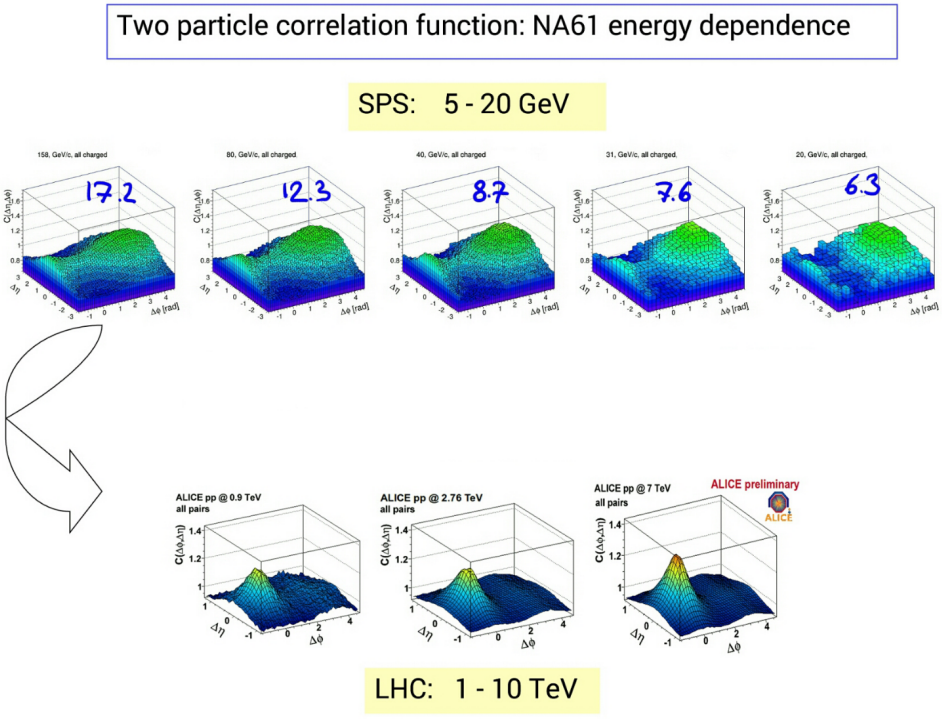

Figure 16. The correlation function shows monotonic evolution with the collision energy. The height of the saddle at (0,0) at the SPS energies and the peak at (0,0) at LHC increase with collision energy.

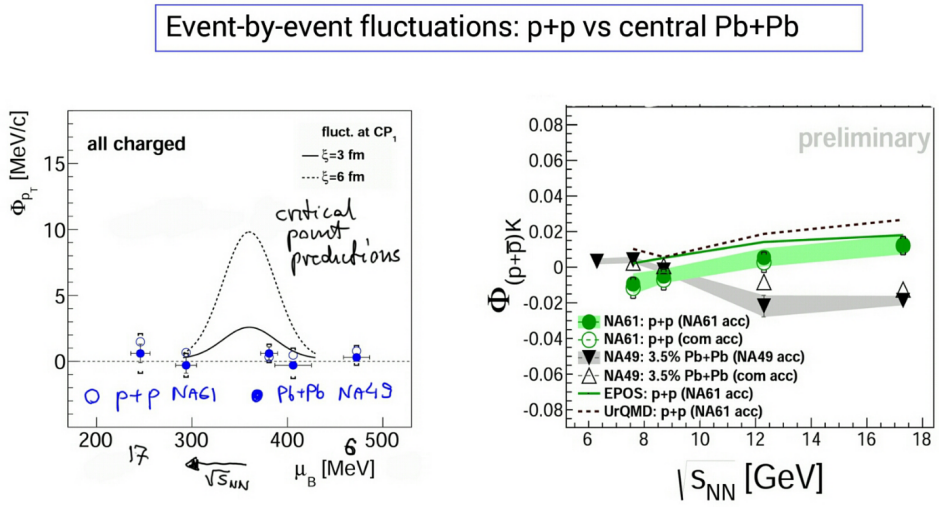

Figure 17. Properly normalized transverse momentum (the left plot) and chemical (the right plot) event-by-event fluctuations are similar in inelastic p+p interactions and central Pb+Pb collisions in the SPS energy range. The largest differences are observed for the relative [kaon, proton] fluctuations (the right plot).

4 Neutrinos

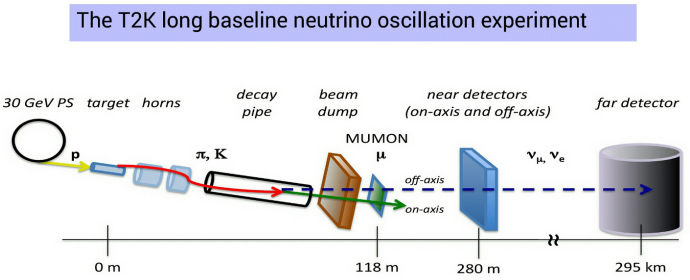

Figure 18. The NA61/SHINE measurements for neutrino physics are motivated by the question how neutrinos change their identities when flying across Japan. In order to answer this question the T2K long baseline neutrino experiment [15] sends a neutrino beam from the J-PARC accelerator at the east coast of Japan to the Kamiokande far detector at the west coast and compares identified neutrino fluxes at the both locations. In order to improve information on the initial flux NA61/SHINE uses a proton beam at the same momentum as in T2K (31 GeV/c) and measures the flux of hadrons from the T2K replica target (90 cm long graphite cylinder) and also from a thin carbon target.

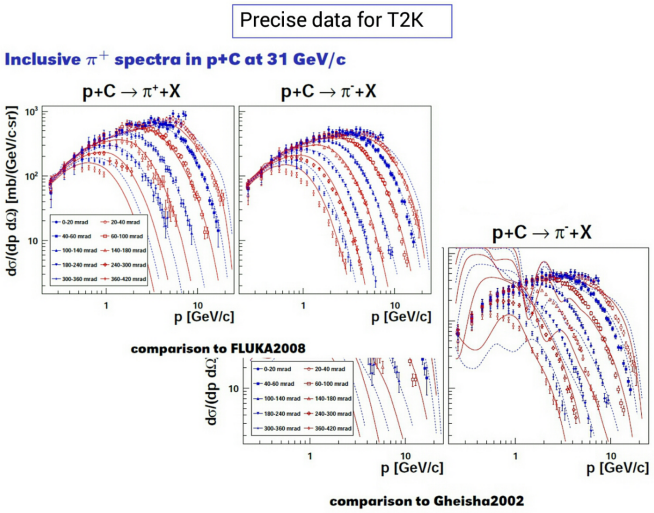

Figure 19. The majority of neutrinos in the T2k beam result from decays of pions. The NA61/SHINE measurements of pion spectra in p+C interactions at 31 GeV/c [16] are necessary to fit models of primary interactions in the T2K target [17].

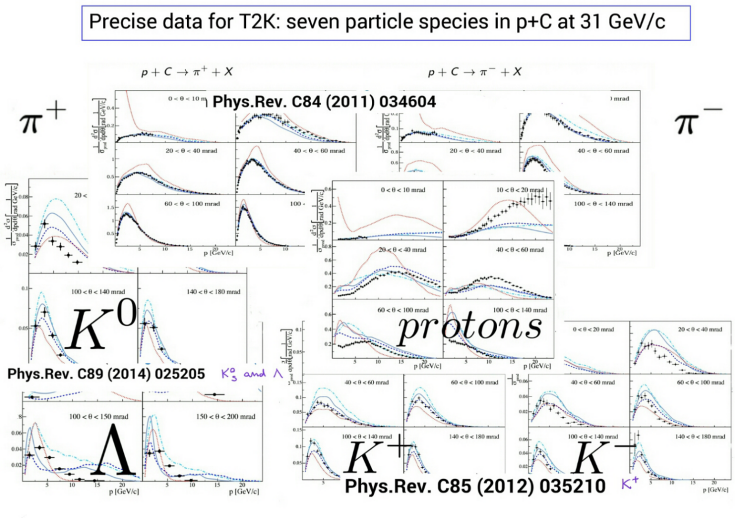

Figure 20. In order to further improve the calculations of the initial neutrino flux measurements of other hadrons abundantly produced in p+C interactions at 31 GeV/c were performed by NA61/SHINE [17–19].

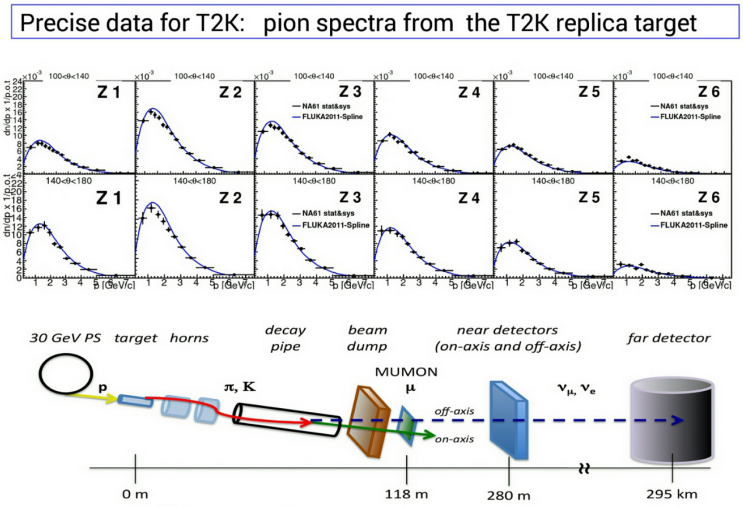

Figure 21. In parallel the flux of identified hadrons from the T2K replica target was measured [20]. The flux is presented separately for six longitudinal sections of the target (Z1-Z6). NA61/SHINE plans to perform similar measurements for the Femilab neutrino experiments [21].

5 Cosmic rays

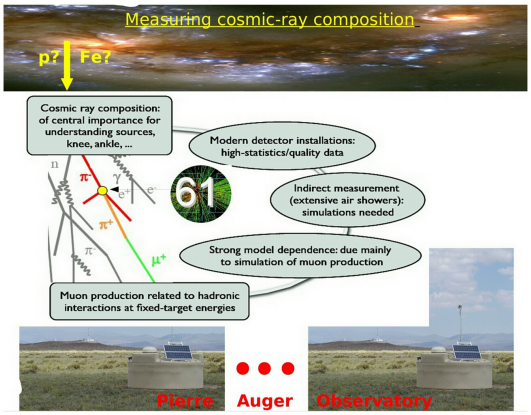
Measuring cosmic-ray composition
p?
Fe?
Cosmic ray composition: of central importance for understanding sources, knee, ankle, ...
Modern detector installations: high-statistics/quality data
Indirect measurement (extensive air showers): simulations needed
Strong model dependence: due mainly to simulation of muon production
Muon production related to hadronic interactions at fixed-target energies
61
Pierre
Auger
Observatory

Figure 22. The NA61/SHINE measurements for cosmic ray physics are motivated by the question of the origin of very high energy cosmic rays. In order to find the answer the Pierre Auger Observatory [22] measures properties of extensive air showers (EAS) at the ground level. These results are then extrapolated back to the primary interactions of cosmic ray particles with air nuclei aiming to extract the cosmic ray energy spectrum and composition. To reduce model depedence of the extrapolation NA61/SHINE measured π^-+C interactions at 158 and 350 GeV/c. Note that pions are the most abundant hadrons in EAS and carbon nuclei can well mimic air nuclei.

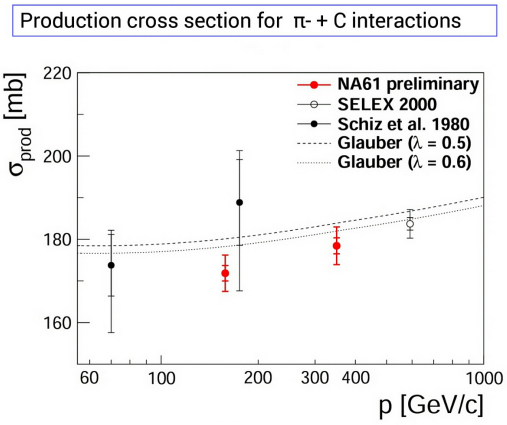

Figure 23. Precise measurements of the production cross section for π^-+C interactions allow to improve the knowledge about the probability of pion-air interactions in EAS [2].

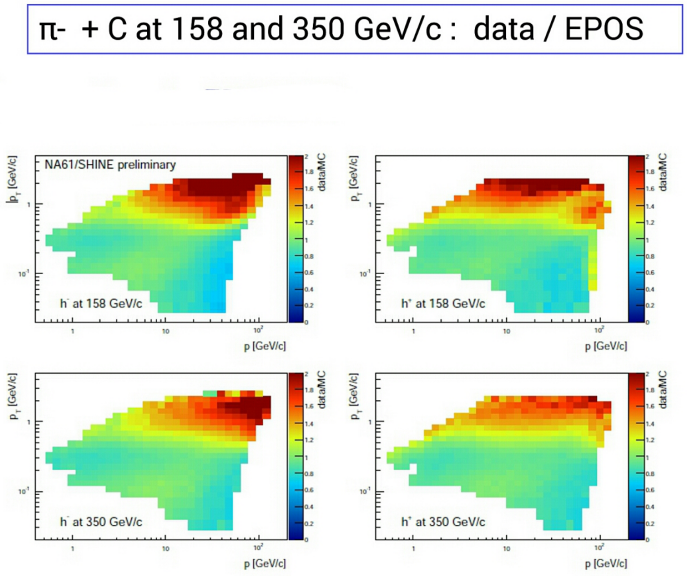

Figure 24. Double-differential spectra of charged hadrons produced in π^-+C interactions [23] serve as an input for fitting models used in EAS simulations.

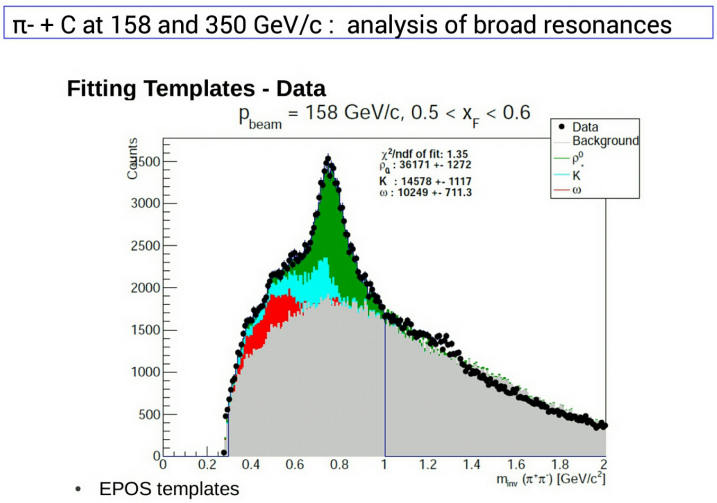

Figure 25. Also production of leading ρ^0 mesons is important for the EAS simulations. Shapes (templates) of invariant mass spectra resulting from decays of various resonances are calculated using the NA61/SHINE simulation chain. Then the normalization of the templates is fitted to reproduce the spectrum measured by the experiment [2] and to extract the resonance yields.

Acknowledgements This work was supported by the National Science Centre of Poland (grant UMO-2012/04/M/ST2/00816) and the German Research Foundation (grant GA 1480/2-2).

References

[1] N. Abgrall *et al.* [NA61 Collaboration], JINST **9**, P06005 (2014) [arXiv:1401.4699 [physics.ins-det]].
[2] N. Abgrall *et al.* [NA61 Collaboration], CERN-SPSC-2014-031; SPSC-SR-145
[3] M. Gazdzicki, M. I. Gorenstein and P. Seyboth, Int. J. Mod. Phys. E **23**, 1430008 (2014) [arXiv:1404.3567 [nucl-ex]].
[4] W. Broniowski, M. Rybczynski and P. Bozek, Comput. Phys. Commun. **180**, 69 (2009) [arXiv:0710.5731 [nucl-th]].
[5] N. Abgrall *et al.* [NA61/SHINE Collaboration], Eur. Phys. J. C **74**, 2794 (2014) [arXiv:1310.2417 [hep-ex]].
[6] V. Uzhinsky, arXiv:1308.0736 [hep-ph].
[7] V. Uzhinsky, arXiv:1109.6768 [hep-ph].
[8] V. Uzhinsky, arXiv:1107.0374 [hep-ph].
[9] V. Uzhinsky, arXiv:1404.2026 [hep-ph].
[10] V. Y. Vovchenko, D. V. Anchishkin and M. I. Gorenstein, Phys. Rev. C **90**, 024916 (2014) [arXiv:1407.0629 [nucl-th]].
[11] V. Y. Vovchenko, D. V. Anchishkin and M. I. Gorenstein, arXiv:1408.5493 [nucl-th].
[12] M. Praszalowicz, Phys. Rev. D **87**, no. 7, 071502 (2013) [arXiv:1301.4647 [hep-ph]].
[13] C. Alt *et al.* [NA49 Collaboration], Phys. Rev. C **77**, 024903 (2008) [arXiv:0710.0118 [nucl-ex]].
[14] S. V. Afanasiev *et al.* [NA49 Collaboration], Phys. Rev. C **66**, 054902 (2002) [nucl-ex/0205002].
[15] K. Abe *et al.* [T2K Collaboration], Nucl. Instrum. Meth. A **659**, 106 (2011) [arXiv:1106.1238 [physics.ins-det]].
[16] N. Abgrall *et al.* [NA61/SHINE Collaboration], Phys. Rev. C **84**, 034604 (2011) [arXiv:1102.0983 [hep-ex]].
[17] A. Korzenev [NA61/SHINE Collaboration], PoS EPS **-HEP2013**, 520 (2013) [arXiv:1311.5719 [nucl-ex]].
[18] N. Abgrall *et al.* [NA61/SHINE Collaboration], Phys. Rev. C **89**, no. 2, 025205 (2014) [arXiv:1309.1997 [physics.acc-ph]].
[19] N. Abgrall *et al.* [NA61/SHINE Collaboration], Phys. Rev. C **85**, 035210 (2012) [arXiv:1112.0150 [hep-ex]].
[20] N. Abgrall *et al.* [NA61/SHINE Collaboration], Nucl. Instrum. Meth. A **701**, 99 (2013) [arXiv:1207.2114 [hep-ex]].
[21] S. Johnson et al. [NA61/SHINE Collaboration], CERN-SPSC-2014-032; SPSC-P-330-ADD-7.
[22] J. Abraham *et al.* [Pierre Auger Collaboration], Nucl. Instrum. Meth. A **523**, 50 (2004).
[23] M. Unger [NA61/SHINE Collaboration], EPJ Web Conf. **52**, 01009 (2013) [arXiv:1305.5281 [nucl-ex]].